

# Designing UNICORN: a Unified Benchmark for Imaging in Computational Pathology, Radiology, and Natural Language

Michelle Stegeman<sup>a,\*</sup>, Lena Philipp<sup>b,\*</sup>, Fennie van der Graaf<sup>b,\*</sup>, Marina D’Amato<sup>a,\*</sup>, Clément Grisi<sup>a,c,\*</sup>, Luc Bultjes<sup>b,\*</sup>, Joeran S. Bosma<sup>b,\*</sup>, Judith Lefkes<sup>a,c,\*</sup>, Rianne A. Weber<sup>b,\*</sup>, James A. Meakin<sup>b</sup>, Thomas Koopman<sup>d,e</sup>, Anne Mickan<sup>b</sup>, Mathias Prokop<sup>b</sup>, Ewoud J. Smit<sup>b</sup>, Geert Litjens<sup>a,c</sup>, Jeroen van der Laak<sup>a</sup>, Bram van Ginneken<sup>b</sup>, Maarten de Rooij<sup>b</sup>, Henkjan Huisman<sup>b</sup>, Colin Jacobs<sup>b</sup>, Francesco Ciompi<sup>a,†</sup>, Alessa Hering<sup>b,†,✉</sup>, and on behalf of the UNICORN consortium<sup>◇</sup>

<sup>a</sup>Department of Pathology, Radboud University Medical Center, Nijmegen, The Netherlands

<sup>b</sup>Department of Medical Imaging, Radboud University Medical Center, Nijmegen, The Netherlands

<sup>c</sup>Oncode Institute, Utrecht, the Netherlands

<sup>d</sup>Informatics Institute, Faculty of Science, University of Amsterdam, Amsterdam, The Netherlands

<sup>e</sup>Departments of Biomedical Engineering and Physics, University Medical Center Amsterdam, Amsterdam, The Netherlands

\*These authors contributed equally to this work and may be listed in any order.

†These authors contributed equally to this work.

◇The consortium author lists are provided in the Consortium Authors section.

✉Corresponding author: Alessa.Hering@radboudumc.nl

## Abstract

**Background** Medical foundation models show promise to learn broadly generalizable features from large, diverse datasets. This could be the base for reliable cross-modality generalization and rapid adaptation to new, task-specific goals, with only a few task-specific examples. Yet, evidence for this is limited by the lack of public, standardized, and reproducible evaluation frameworks, as existing public benchmarks are often fragmented across task-, organ-, or modality-specific settings, limiting assessment of cross-task generalization.

**Methods** We introduce UNICORN, a public benchmark designed to systematically evaluate medical foundation models under a unified protocol. UNICORN spans 20 tasks across radiology, pathology, and clinical text, covering classification, detection, segmentation, regression, and vision-language generation. To isolate representation quality, we built the benchmark on a novel two-step framework that decouples model inference from task-specific evaluation based on standardized few-shot adaptation. As a central design choice, we constructed indirectly accessible sequestered test sets derived from clinically relevant cohorts, along with standardized evaluation code and a submission interface on an open benchmarking platform. Performance is aggregated into a single UNICORN Score, a new metric that we introduce to support direct comparison of foundation models across diverse medical domains, modalities, and task types.

**Results** The UNICORN test dataset includes data from more than 2,400 patients, including over 3,700 vision cases and over 2,400 clinical reports collected from 17 institutions across eight countries. The benchmark spans eight anatomical regions and four imaging modalities. Both task-specific and aggregated leaderboards enable accessible, standardized, and reproducible evaluation. A baseline implementation based on publicly available models and equipped with lightweight adaptors successfully executes across all tasks and produces a UNICORN score of 0.378.

**Conclusion** By standardizing multi-task, multi-modality assessment, UNICORN establishes a foundation for reproducible benchmarking of medical foundation models. Data, baseline methods, and the evaluation platform are publicly available via [unicorn.grand-challenge.org](https://unicorn.grand-challenge.org).

# 1 Introduction

The integration of artificial intelligence into diagnostic workflows is growing [1], which causes increasing interest in standardized evaluation frameworks to enable transparent and reproducible comparison of models across diseases, imaging domains, and clinical settings. Over the past decade, public challenges have increasingly become a reference tool to benchmark deep learning models in medical imaging. Since their inception, most challenges have followed a “one-to-one” design, where one algorithm competes on a single, narrowly defined task, typically restricted to a single anatomical region, data modality, or output target. Examples of challenges include PI-CAI [2] for tumor detection in prostate MRI, TIGER [3] for quantification of tumor-infiltrating lymphocytes in breast cancer digital pathology, and LUNA16 [4] for the detection of pulmonary nodules in CT scans. These challenges have accelerated task-specific progress in model development and established widely used evaluation protocols.

Foundation models introduce a fundamentally different paradigm, centered around broad, pre-trained encoders learned from large-scale medical data spanning multiple domains, modalities, anatomical regions, and disease contexts, typically using self- or weakly supervised objectives [5, 6, 7]. Rather than learning patterns that are highly optimized for a single, predefined task, limited to one clinical application, foundation models produce rich, general purpose representations that capture generic features across diverse inputs. These representations can be adapted to new downstream tasks with minimal additional training, reducing annotation needs and improving robustness across scanners, institutions, and populations.

In medical imaging, several foundation models have been developed for specific domains, such as CTransPath [8], Phikon [9], and UNI [10] for digital pathology, CT-FM [11] and Foundation Model for Cancer-Imaging Biomarkers [12] for CT radiology, and USFM [13] for ultrasound. In parallel, a growing body of work in multimodal learning has explored approaches for combining medical images with corresponding text reports to learn from both sources jointly. These approaches enable applications such as visual question answering (VQA), report generation, and bidirectional image-text retrieval. Resulting vision language models (VLMs) include MedCLIP [14], Med-Gemini [15], and Med-PaLM [16], along with domain-focused variants such as CT-CLIP [17] and Merlin [18] for CT, ELIXR [19] and BioViL-T [20] for X-ray, and Quilt-1M [21] and CONCH [22] for pathology.

Because these foundation models produce generic representations that can be adapted to many downstream tasks, evaluating their performance requires a shift from task-specific benchmarks toward a “one model-many tasks” evaluation that measures generalization across diverse domains, modalities, and task types.

Several recent benchmarking initiatives have enabled systematic, broad, multi-organ, and multimodal evaluation in radiology. This includes the Medical Segmentation Decathlon [23], FLARE [24], AMOS [25], and CHAOS [26] for segmentation, Learn2Reg [27] for registration and MOOD [28] for out-of-distribution detection. Complementary efforts address the systematic evaluation of medical foundation models. These include the clinical benchmark of public self-supervised pathology encoders [29], a real-world dataset and benchmark for foundation model adaptation in medical-image classification [30], eva, an evaluation framework for pathology foundation models [31], and FairMedFM [32], examining fairness across modalities for both classification and segmentation. Together, these efforts substantially expand datasets and anatomical diversity while enabling evaluation across a range of specific task types such as classification, segmentation, registration, or out-of-distribution detection.

In natural language processing, large language models (LLMs) are evaluated in an open and reproducible manner using benchmarks such as the HuggingFace Open LLM Leaderboard [33], which covers diverse domains including mathematics, medicine, and geometry. Complementary medical language benchmarks such as DRAGON [34], HealthBench [35], and MedHELM [36] further demonstrate how broad, standardized evaluation frameworks can support systematic, transparent, and comparable assessment of model capabilities in clinical language tasks.

Although many existing initiatives provide systematic and high-quality evaluations for specific areas, covering a range of tasks, modalities, or domains, they remain focused on a subgroup. Therefore, assessing the broad capabilities of foundation models is fragmented across multiple benchmarks with heterogeneous evaluation protocols and metrics, which lack comparability and consistency. As a result, the field still lacks a publicly available, single, unified framework capable of evaluating medical foundation models simultaneously across multiple tasks, modalities, and domains using standardized, consistent, and reproducible metrics. In addition, evaluation data should be strictly sequestered to prevent data

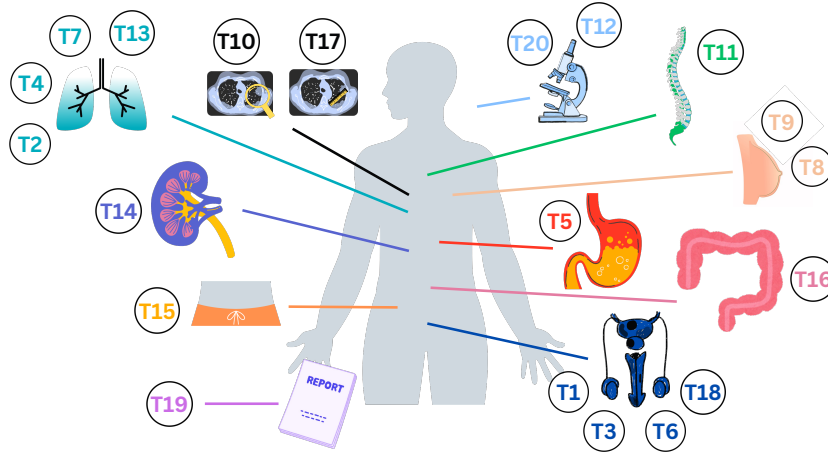


Figure 1: **Overview of the 20 UNICORN benchmark tasks.** The benchmark includes 20 tasks, of which 15 focused on eight different anatomic regions, whereas the remaining five are broad-scope tasks that span multiple regions or represent specific medical processes.

leakage in model training and ensure the validity of the reported performance.

To address this gap, we introduce a Unified beNchmark for Imaging in COmputational pathology, Ra-diology, and Natural language (UNICORN), a multi-task, multi-domain, and multi-modality benchmark designed to evaluate medical foundation models within a single, standardized framework. UNICORN integrates 20 tasks spanning radiology, digital pathology, clinical language understanding, and vision-language generation. All tasks use sequestered test sets derived from real-world clinical cohorts to ensure unbiased and reproducible evaluation. Several tasks build upon established public challenges, preserving clinically validated reference standards and enabling comparison with task-specific models.

A core component of UNICORN is a new few-shot evaluation framework that decouples foundation-model inference from lightweight task-specific adaptation, thereby isolating the generality and quality of learned representations. This design reflects the constraints of clinical data curation, where labeled data are scarce, and provides a consistent and reproducible basis for comparing heterogeneous models across tasks and modalities.

In summary, UNICORN advances the field in two primary ways:

1. It establishes the first unified benchmark for evaluation of medical foundation models across diverse tasks and modalities, offering an open and reproducible framework for assessing generalization at scale; and
2. To ensure consistent and reproducible comparison of heterogeneous model architectures, UNICORN introduces a two-step evaluation strategy that isolates image representation quality from task-specific adaptation, implemented within a shared, fully hosted infrastructure on Grand Challenge.

## 2 Data overview

Medical foundation models are designed to generalize across anatomical regions, task types, modalities, and clinical domains, rather than being optimized for narrow, task-specific applications. To evaluate this capability realistically and systematically, UNICORN introduces a diverse set of 20 clinically motivated tasks, spanning radiology, pathology, and natural language. Of these 20 tasks, 15 are specific to anatomical regions, while the remaining five are broad-scope tasks spanning multiple anatomical regions, or representing general clinical processes (Figure 1). Across the 15 region-specific tasks, eight anatomical regions are represented: lung, hip, kidney, prostate, colon, stomach, breast, and spine. UNICORN spans multiple task types to assess whether a single pre-trained model can support heterogeneous clinical objectives using a shared representation. Across 20 tasks, UNICORN includes eight classification tasks, four detection tasks, three regression tasks, three segmentation tasks, one named entity recognition task, and one caption generation task. This diversity requires algorithms to handle both global semantic reasoning and spatially grounded predictions, as well as language understanding. UNICORN further evaluates generalization across modalities and clinical domains. Of the 20 tasks, 11 are vision-only tasks, eight are

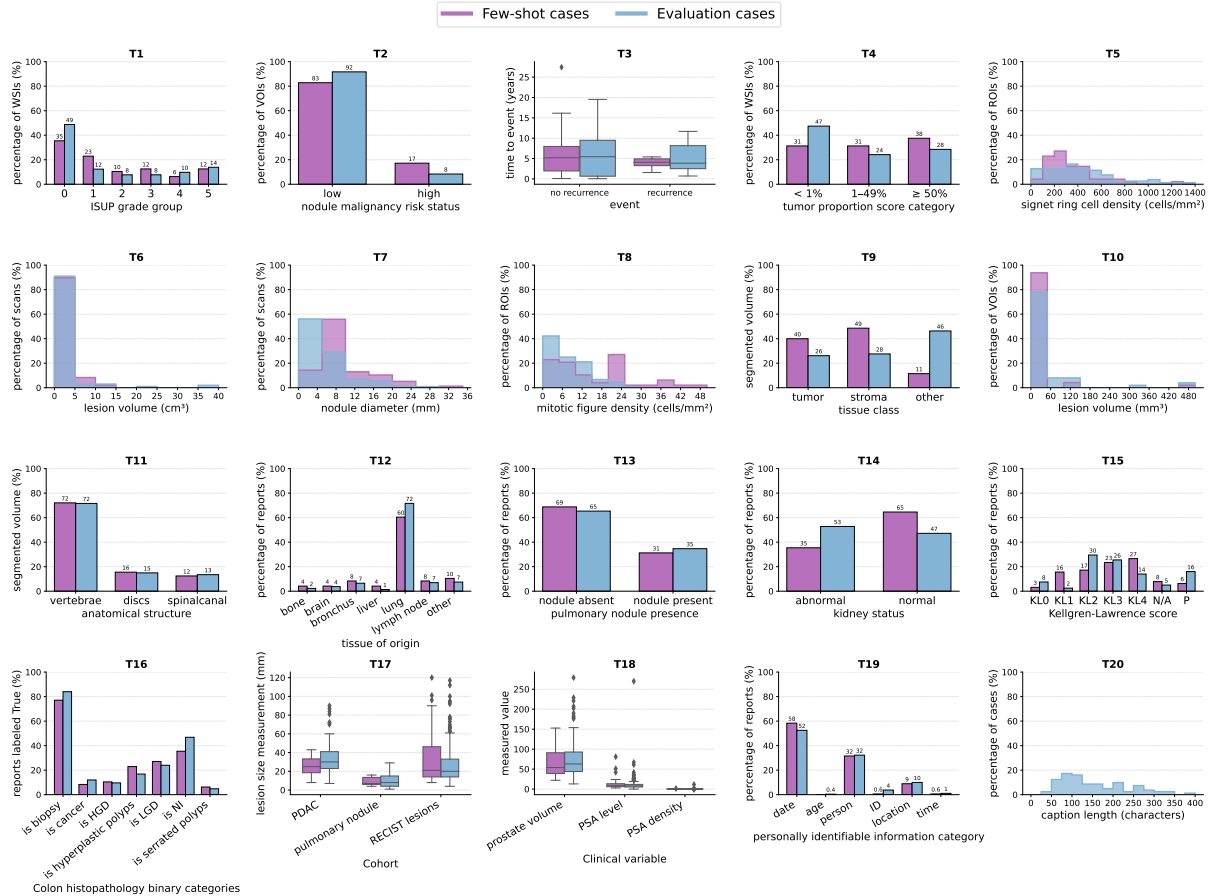


Figure 2: **Reference labels in the UNICORN validation set.** For classification tasks, **T1**, **T2**, **T4**, **T12-T16**, bar charts show the proportion of cases per label. For **T16**, which contains seven independent binary labels, each bar represents the proportion of reports labeled True, with the remainder corresponding to the proportion of False labels. Regression tasks, **T3**, **T17**, **T18**, are summarized with boxplots of target values, detection tasks, **T5-T8**, with histograms of object counts, and segmentation tasks, **T9-T11**, with bar charts showing either the proportion of each class for multiclass tasks, or the proportion of object volume for single class tasks. For named entity recognition, **T19**, bars show the distribution of target categories, and for caption generation, **T20**, the distribution of caption lengths is shown, few-shots are not available for this task.

language-only tasks, and one is a vision-language task. In terms of domain, UNICORN covers 10 radiology tasks, nine pathology tasks, and one joint task spanning radiology and pathology. This balanced distribution allows for systematic evaluation of whether a foundation model learns representations that transfer across domains and modalities under a unified protocol. An overview of all tasks, including task type, modality, domain, and evaluation metrics, is provided in Table 1, with detailed task descriptions available in Supplemental 1.

Beyond task diversity, UNICORN intentionally reflects the heterogeneous and often imbalanced nature of real-world clinical data. Figure 2 summarizes label distributions across all 20 tasks in the UNICORN validation set, showing substantial variation in class prevalence, outcome frequencies, and annotation density. For tasks that support few-shot adaptation, distributions are shown separately for few-shot examples and evaluation case data, illustrating the degree to which the examples reflect the tasks’ evaluation cases. These label distributions ensure that performance on UNICORN reflects clinically realistic label distribution and enable systematic evaluation of a model’s ability to generalize across diverse, real-world clinical tasks.

UNICORN datasets were sourced from 17 institutions across eight countries and were collected from sequestered data of real-world clinical cohorts. All data were fully anonymized before inclusion. The data were previously used in challenges or clinical projects, where ethical approval or consent waivers were obtained.

To facilitate algorithm development, Table S1 summarizes for each UNICORN task a related publicly available dataset, including usage license, public links, and associated publications. While these datasets may be used for pertaining or local experimentation, all UNICORN test data is sequestered.

Table 1: Overview of the tasks in the UNICORN challenge. *AUROC* = area under the receiver operating characteristic curve, *CLS* = classification, *DET* = detection, *GEN* = caption generation, *H&E* = Hematoxylin and Eosin, *IHC* = immunohistochemistry, *ISUP* = International Society of Urological Pathology, *MIXED* = radiology and pathology, *NER* = named entity recognition, *NSCLC* = non-small cell lung cancer, *PATH* = Pathology, *PSA* = prostate-specific antigen, *RAD* = Radiology, *REG* = regression, *ROIs* = regions of interest, *SEG* = segmentation, *WSI* = whole-slide image.

ID	Name	Type	Modality	Metric	Cases (few-shot / validation / test)	Time limit (min)
<b>Vision tasks</b>						
T1	ISUP scoring in H&E prostate biopsies	CLS	PATH	Quadratic weighted kappa	48 / 195 / 113	10
T2	Lung nodule malignancy in CT	CLS	RAD	AUROC	64 / 108 / 533	5
T3	Time to biochemical recurrence in H&E prostatectomies	REG	PATH	Censored c-index	48 / 49 / 521	25
T4	Tumor proportion score in NSCLC IHC WSI	CLS	PATH	Quadratic weighted kappa	48 / 116 / 474	10
T5	Signet ring cells in H&E ROIs of gastric cancer	DET	PATH	F1 score	48 / 79 / 348	10
T6	Clinically significant prostate cancer in MRI	DET	RAD	Average of AUROC and AP	48 / 100 / 400	10
T7	Lung nodule detection in thoracic CT	DET	RAD	Sensitivity	48 / 83 / 83	5
T8	Mitotic figures in breast cancer H&E ROIs	DET	PATH	F1 score	48 / 180 / 400	10
T9	Tumor and stroma segmentation in breast H&E	SEG	PATH	Dice	48 / 24 / 33	5
T10	Universal lesion segmentation in CT ROIs	SEG	RAD	Dice, long- and short-axis errors	48 / 50 / 725	10
T11	Anatomical segmentation in lumbar spine MRI	SEG	RAD	Dice	48 / 48 / 97	10
<b>Language tasks</b>						
T12	Histopathology sample origin	CLS	PATH	Unweighted kappa	48 / 215 / 297	240/240*
T13	Pulmonary nodule presence	CLS	RAD	AUROC	48 / 300 / 200	120/240*
T14	Kidney abnormality	CLS	RAD	AUROC	48 / 125 / 183	120/240*
T15	Hip Kellgren-Lawrence scoring	CLS	RAD	Unweighted kappa	32 / 100 / 108	120/240*
T16	Colon histopathology diagnosis	CLS	PATH	Macro AUROC	48 / 250 / 500	120/240*
T17	Lesion size measurements	REG	RAD	R SMAPE	48 / 242 / 298	120/240*
T18	Prostate volume and PSA (density)	REG	RAD	R SMAPE	48 / 250 / 500	120/240*
T19	Report anonymization	NER	MIXED	Weighted F1	48 / 200 / 400	120/240*
<b>Vision-Language task</b>						
T20	WSI captioning	GEN	PATH	BLEU-4, ROUGE-L, METEOR, CIDER, BERTscore	0 / 81 / 310	25

\* Time limit given as validation/test.

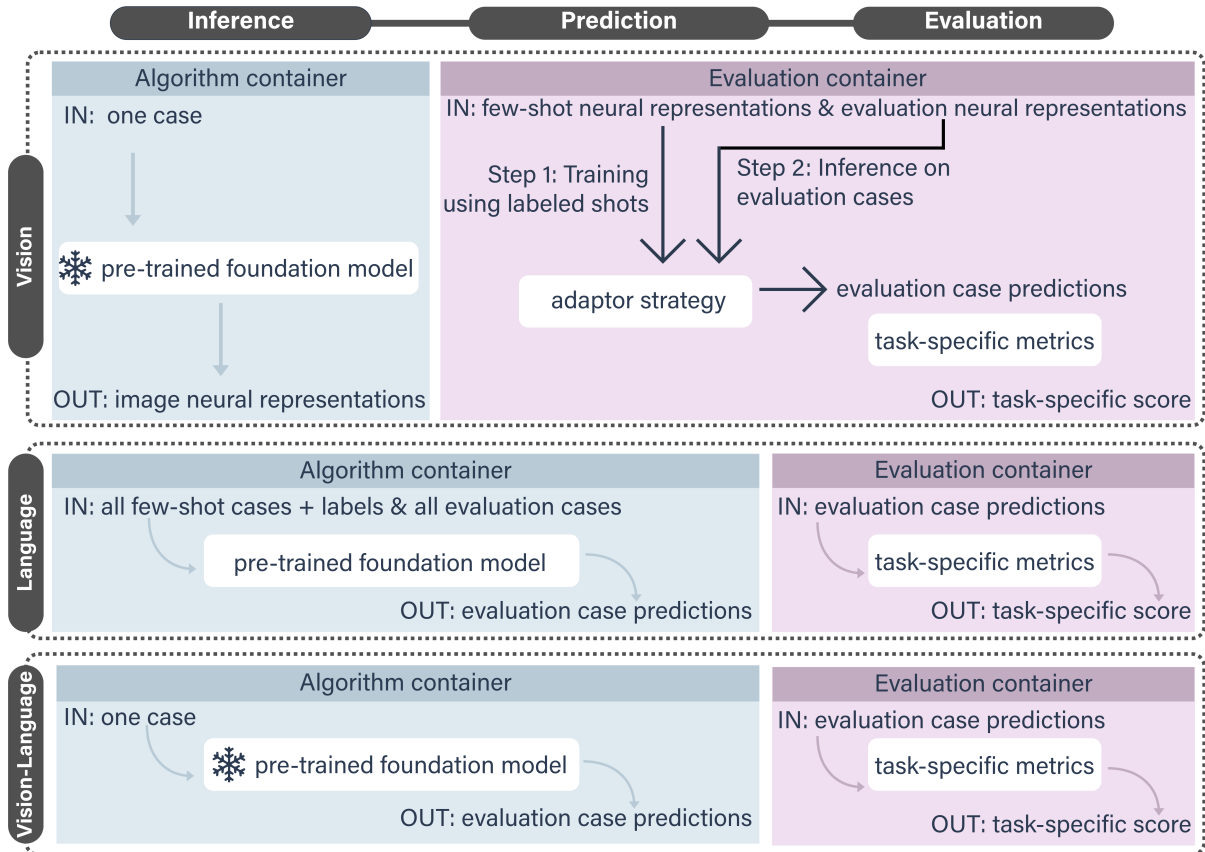


Figure 3: **UNICORN benchmarking pipeline** The pipeline is structured vertically from data storage to metrics reporting, with modality-specific differences shown horizontally for vision, language, and vision–language. *Vision tasks*: Each case is processed by the Algorithm container to extract generic representations using pre-trained foundation models. These representations are passed to the Evaluation container, where a lightweight adaptor trained on labeled few-shot examples produces task-specific predictions and computes evaluation metrics. *Language tasks*: All labeled few-shot cases and evaluation cases are together provided to the Algorithm container, which generates predictions that are evaluated in the Evaluation container. *Vision-language task*: Each case is processed individually by the Algorithm container, which uses the textual task description to generate a textual prediction that is evaluated in the Evaluation container. For all tasks, the resulting metrics are reported on their respective leaderboards on Grand Challenge.

### 3 UNICORN Framework

As illustrated in Figure 3, the UNICORN benchmark provides a systematic and standardized approach for evaluating medical foundation models across vision, language, and vision–language modalities. The benchmark process follows a unified pipeline that spans data storage, algorithm inference, task-specific predictions, task-specific metric computation, and leaderboard reporting. This structure enables consistent evaluation across modalities while allowing modality-specific variations at each stage.

The entire benchmarking process is performed on the Grand Challenge platform [37]<sup>1</sup>, where a standardized two-step architecture was implemented, separating foundation model inference from task-specific evaluation.

The first step, the *Algorithm*, is a collection of all dependencies and code required for execution, provided by users as a container image. Optionally, alongside a packaged model archive containing one or more pre-trained foundation models. The second step, the *Evaluation container*, is maintained by the UNICORN organizers and performs task-specific adaptation and computes task-specific evaluation metrics.

<sup>1</sup>grand-challenge.org

## Data Storage

All data are organized in sequestered archives on the Grand Challenge platform to ensure secure and unbiased evaluation. Each archive item contains a single case for vision and vision-language tasks, or a combined set of reports for language tasks. Depending on the task, a case may represent a patient examination, a whole-slide image, or a specific region of interest (see Supplemental 1 for task definitions). For vision and vision-language tasks, cases are provided individually to the Algorithm container without revealing whether they belong to the few-shot or evaluation set. For language tasks, all cases, including both the labeled few-shot examples and the evaluation cases requiring prediction, are provided to the algorithm at once. This design ensures consistent evaluation across modalities while maintaining the integrity of hidden test data.

## Algorithm Inference

The Algorithm container autonomously processes each case provided by the platform. For vision and vision-language tasks, it extracts generic representations suitable for downstream adaptation, whereas for language tasks, it generates task-specific predictions. All required steps, such as preprocessing, prompting, and language-specific tuning steps, are executed within the container without internet access to ensure data security. Each archive item is accompanied by a task configuration file specifying domain, modality, task type, and output shape requirements. Publicly available templates and baseline resources relevant to this workflow are summarized in Supplemental 3.

**Vision tasks** Each vision task has multiple archive items, each archive item containing one case. Cases are processed one at a time to produce generic representations suitable for downstream adaptation. For dense prediction tasks, such as segmentation and detection, multiple patch-level representations may be extracted to capture spatially resolved information. In contrast, case-level tasks, such as classification and regression, require aggregation into a single representation per case, thereby aligning the Algorithm output with the granularity of the reference labels.

**Language tasks** For each language task, a single archive item contains all labeled few-shot cases along with the evaluation cases. The algorithm generates task-specific predictions through a complete pipeline that may include preprocessing (e.g., text-normalization), the use of a pre-trained foundation model, fine-tuning or prompting on the few-shot dataset, and postprocessing.

**Vision-language tasks** Each vision-language archive contains a single case, which is processed independently by the Algorithm container to generate a task-specific prediction. The task description provided configuration file may be used to guide prediction, and postprocessing can include translation into the target label language.

## Evaluation

The Evaluation container transforms the Algorithm outputs into task-specific performance scores and computes the metrics used for leaderboard ranking. For all tasks, predictions generated or derived from the Algorithm output are compared against sequestered reference labels to assess the task-specific performance (see Table 1). By centralizing all evaluation in a single container, UNICORN ensures reproducible and consistent assessment across all submissions, modalities, and domains. For language and vision-language tasks, the Algorithm directly outputs task-specific predictions in the required output format. These are passed unchanged to the Evaluation container, which computes task-specific metrics against the sequestered reference labels.

For vision tasks, task-specific metrics cannot be computed directly from the Algorithm output, as the output consists of generic representations, rather than task-specific predictions. To transform these generic representations into task-specific predictions, a user-selected adaptor strategy is trained using the labeled few-shot representations. These strategies range from non-parametric methods, such as k-nearest neighbors, to lightweight learning-based approaches. UNICORN provides a set of standard baseline adaptors, and community contributions are made by uploading new adaptors to the official UNICORN evaluation repository<sup>2</sup> on GitHub via pull requests. All approved strategies are made publicly available

---

<sup>2</sup>[https://github.com/DIAGNijmegen/unicorn\\_eval](https://github.com/DIAGNijmegen/unicorn_eval)

through the GitHub repository and on the Grand Challenge platform to promote transparency and ensure that the broader community benefits from the newly developed adaptor strategies.

### 3.1 UNICORN Score

Evaluating the overall foundational characteristics of foundation models across multiple tasks and modalities requires a unified metric that summarizes overall performance. Since each task in UNICORN uses a different evaluation measure, ranging from Dice similarity to AUROC and mean absolute error, these values must be made comparable to assess how well a foundation model performs overall. The **UNICORN Score** addresses this need by combining task-specific metrics into a single, standardized measure of generalizability.

Performance on each downstream task was first computed using its task-specific metric (Table 1). To aggregate results across heterogeneous metrics and task types, all scores were normalized to a common 0–1 range using a consistent scaling scheme. For each task  $n$ , the normalized score  $t_n$  was calculated as

$$t_n = \frac{S_n - S_n^{\text{ref}}}{S_n^{\text{max}} - S_n^{\text{ref}}}, \quad (1)$$

where  $S_n$  denotes the raw task-specific score,  $S_n^{\text{ref}}$  denotes the performance of a minimal reference model (e.g., a majority-class predictor for classification tasks), and  $S_n^{\text{max}}$  represents the maximum achievable value of the corresponding metric. This normalization ensures all metrics are on a common scale. Using a minimal reference model anchors normalization at a meaningful lower bound, ensuring that scores reflect improvement over trivial solutions.

The overall UNICORN Score,  $S_{\text{UNICORN}}$ , is defined as the mean of the normalized scores across all  $N = 20$  tasks:

$$S_{\text{UNICORN}} = \frac{1}{N} \sum_{n=1}^N t_n. \quad (2)$$

All tasks were weighted equally to reflect a uniform, cross-task generalization, rather than prioritizing specific domains or dataset sizes. This aggregated score provides an interpretable measure of how well a foundation model generalizes across diverse tasks and modalities. Domain-specific UNICORN Scores (for pathology, radiology, and language) were computed analogously by averaging normalized scores within each domain. Task-specific normalization constants are provided in Supplemental 2.4.

### 3.2 UNICORN Phases

UNICORN consists of four sequential phases.

First, public example datasets [38] were released during the off-platform development phase to support local prototyping and to ensure compatibility with the container-based execution used in later stages.

Second, a non-scored check phase used a small, carefully selected dataset containing edge cases, e.g., the largest image from the cohort, to verify that each user’s Algorithm container image could execute end-to-end within time on the Grand Challenge platform. Successful completion of the check phase was required for entry into subsequent phases.

Third, the validation phase provided users with intermediate performance feedback on sequestered data. To support detailed evaluation, task-specific leaderboards were made available, alongside three domain/ modality-specific combined leaderboards (pathology–vision, radiology–vision, and language), and an all-tasks leaderboard covering all 20 tasks. The all-tasks leaderboard is the primary endpoint, while the domain/ modality-specific leaderboards enable evaluation of more specialized algorithms. During validation, each user was limited to a total of six successful submissions per task: three to each task-specific leaderboard, two per combined leaderboard, and one to the all-tasks leaderboard.

Finally, the test phase consisted of a single opportunity on sequestered data, either to the all-tasks leaderboard or to each of the combined leaderboards. Additional information about phases is provided in Supplemental 2.

## 4 Discussion

The UNICORN challenge has been developed to address the lack of publicly available benchmarks for evaluating medical foundation models across a broad range of tasks, organs, domains, and modalities.

Most existing efforts focus on a single task type, organ system, or modality, which limits the ability to determine a foundation model’s generalization capabilities across clinically diverse settings. UNICORN offers a “one model–many tasks” evaluation: pretrained encoders are compared via few-shot adaptation on 20 tasks across multiple domains, radiology and pathology, and multiple modalities, including vision, language, and vision–language. Their cross-task performance is summarized in a single UNICORN Score under a unified evaluation protocol.

Tasks were selected based on clinical relevance and technical difficulty, with many derived from existing public challenges with expert annotations and demonstrated clinical demand. Rather than simplifying problems by cropping images to predefined regions of interest, UNICORN includes full-resolution whole-slide pathology images and complete CT or MRI scans, introducing real-world complexity such as variable input sizes, multiple lesions per case, and clinically meaningful label uncertainty. In this setting, models must capture spatial structure and long-range context across the entire image or volume, rather than treating isolated patches as independent samples. Because tasks share a common submission interface and evaluation logic, additional datasets, modalities, and task types can be incorporated without changing the overall framework, allowing the benchmark to grow over time with new, clinically motivated tasks.

Building on these real-world constraints, a core design choice was to decouple the frozen encoder from lightweight task-specific adaptation. By extracting generic representations using a frozen decoder, UNICORN evaluates the quality of these representations for reliable performance across tasks, without reliance on complex task-specific tuning pipelines.

To reflect the limited availability of labeled clinical data, adaptation is restricted to few-shot examples, and pretrained weights are not allowed in adaptors. To support local development, reproducibility, and consistent comparison across submissions, public datasets, and an open-source repository providing adaptor implementations and evaluation code are available.

The Grand Challenge platform was expanded to support joint evaluation of diverse tasks by handling multiple data modalities and prediction targets within a unified leaderboard, and enabling adaptor training within the Evaluation container. Whereas a standard challenge setup assumes a single homogeneous task, UNICORN introduces combined leaderboards that aggregate performance across tasks with distinct input types, output structures, and evaluation metrics. This design allows the evaluation of algorithms under a unified protocol despite the diversity of tasks. It supports task-specific leaderboards for debugging and detailed performance analysis, as well as combined leaderboards for assessing cross-task generalization. For combined leaderboards, the performance is summarized by the UNICORN Score. The UNICORN score facilitates comparison between algorithms and simplifies model selection by providing a single summary measure of performance that equally weights all tasks and depends on the chosen reference scores. Its interpretation is complemented by task-wise results, which together provide a complete assessment of performance across tasks.

The design of the UNICORN challenge was shaped by several practical constraints, particularly regarding data availability, computational resources, and architectural flexibility. Although the benchmark covers a broad range of clinically relevant tasks and datasets collected from multiple institutions, most test data was sourced from a single academic center. This limits the ability to assess how well submitted solutions generalize to data from other institutions, scanners, and patient populations. At the same time, because many UNICORN tasks reuse datasets and metrics from earlier challenges, the benchmark creates an opportunity for future work to systematically compare foundation models against strong task-specific baselines by re-evaluating prior challenge-winning models within the UNICORN framework.

To focus on generalizable representations and while respecting computational and storage constraints, case-level classification and regression tasks required a single generic representation at case level. This constrained solutions that depend on dense patch-level outputs or more flexible, task-specific prediction heads at adaptation time. As a result, the benchmark primarily offers meaningful assessments for models that learn strong general-purpose features and can be adapted with minimal supervision, rather than those that depend on heavy task-specific tuning.

In addition, computational limits shaped several aspects of the evaluation protocol. Restrictions on the number of submissions and the maximum execution time per case excluded computationally expensive Algorithms, but were necessary to keep large-scale evaluation feasible. Architectural flexibility was further limited by the use of separate containers for the encoder and adaptor, and pretrained decoders were not supported, which prevented some state-of-the-art task-specific models from being submitted in their original form. While these constraints help ensure that the benchmark remains practically runnable

and focused on encoder quality, they also limit the range of modeling strategies that can currently be assessed within UNICORN.

UNICORN lays the groundwork for future efforts to evaluate generalist foundation models in medical imaging. By enabling standardized, few-shot evaluation across diverse tasks and modalities, it creates the conditions needed to study generalization under realistic clinical constraints. Engagement from over 270 researchers across six continents reflects strong community interest in unified benchmarks and task-agnostic model development. As the benchmark evolves, new tasks, modalities, and centers can be integrated, and comparisons to existing supervised benchmarks can help clarify when foundation models outperform or complement task-specific approaches. In this setting, the UNICORN Score and domain-specific leaderboards together support more efficient model selection and help identify foundation models that generalize well with minimal supervision, particularly valuable in data-scarce clinical environments. By evaluating a single feature extractor across multiple outputs and domains, UNICORN anticipates the move toward consolidated model pipelines and offers guidance for developers and institutions navigating the need for scalable, robust AI systems.

## 5 Conclusion

UNICORN establishes the first large-scale benchmark for evaluating medical foundation models across diverse tasks, modalities, and clinical domains. By providing a standardized few-shot evaluation framework, shared development datasets, and a multi-task infrastructure on Grand Challenge, UNICORN enables reproducible and consistent comparison across models. This benchmark lays essential groundwork for guiding model development, fostering community collaboration, and enabling standardized evaluation that is critical for developing robust, generalizable models suitable for clinical deployment.

## Acknowledgments

This research is supported by multiple public and private funding sources. F.C., M.D.A., and M.S. received funding from the Innovative Medicines Initiative 2 Joint Undertaking under grant agreement No 945358. This Joint Undertaking receives support from the European Union’s Horizon 2020 research and innovation program and EFPIA. [www.imi.europe.eu](http://www.imi.europe.eu). The views expressed are those of the authors only, and neither the IMI JU nor the Commission is liable for any use that may be made of the information contained therein. F.vd.G was funded through a public-private project with funding from the Dutch Research Council (NWO), the Dutch Ministry of Economic Affairs, and MeVis Medical Solutions (Bremen, Germany). L.B. acknowledges support from RadboudAI J.S.B. received funding from HealthHolland (LSHM20103). The collaboration project is co-funded by PPP Allowance awarded by HealthHolland, Top Sector Life Sciences & Health, to stimulate public-private partnerships. Views and opinions expressed are however those of the author(s) only and do not necessarily reflect those of the European Union or European Health and Digital Executive Agency (HADEA). Neither the European Union nor the granting authority can be held responsible for them. R.A.W. received funding from the project ‘OncoFuture: Hybrid AI for Efficient Cancer Diagnosis and Follow-Up Assessment’ with file number NGF.1607.22.032 of the research programme AiNed Fellowship Grants which is (partly) financed by the Dutch Research Council (NWO). For F.C., this publication is part of the project IGNITE with file number 18388 of the research programme Vidi - Applied and Engineering Sciences. Which is (partly) financed by the Dutch Research Council (NWO). For A.H., this publication is part of the project OncoChange with file number 21121 of the research programme Veni - Applied and Engineering Sciences. Which is (partly) financed by the Dutch Research Council (NWO).

## The UNICORN Consortium

Michelle Stegeman<sup>a,\*</sup>, Lena Philipp<sup>b,\*</sup>, Fennie van der Graaf<sup>b,\*</sup>, Marina D’Amato<sup>a,\*</sup>, Clément Grisi<sup>a,c,\*</sup>, Luc Bultjes<sup>b,\*</sup>, Joeran S. Bosma<sup>b,\*</sup>, Judith Lefkes<sup>a,c,\*</sup>, Rianne A. Weber<sup>b,\*</sup>, Alon Vigdorovits<sup>f</sup>, Anindo Saha<sup>b</sup>, Anna-Vibeke Laenkholtm<sup>g,h</sup>, Bogdan Obreja<sup>b</sup>, Clara I. Sánchez Gutiérrez<sup>a,e</sup>, Chris van Run<sup>b</sup>, Christian Roest<sup>i</sup>, David Tellez<sup>a</sup>, Denis Larsimont<sup>j</sup>, Dennis Rouw<sup>k</sup>, Derya Yakar<sup>l,i</sup>, Dieter J.E. Peeters<sup>m,n</sup>, Dré Peeters<sup>b</sup>, Elisabeth Ida Specht Stovgaard<sup>o,p</sup>, Elise M.G. Taken<sup>b</sup>, Ernst Th. Scholten<sup>b</sup>, Gijs Stultiens<sup>b</sup>, Harm van Zeeland<sup>a</sup>, Harry Haynes<sup>q</sup>, Inge M. E. Smit<sup>b</sup>, Iris D. Nagtegaal<sup>a</sup>, Ivan R. Slootweg<sup>a</sup>, Jasper J.

Twilt<sup>b</sup>, Jasper van der Graaf<sup>b</sup>, Jeroen Geerdink<sup>r</sup>, Jeroen Veltman<sup>s</sup>, Job van Susante<sup>t</sup>, Joep Bogaerts<sup>a</sup>, Joey M. A. Spronck<sup>a</sup>, Jos J. Immerzeel<sup>u</sup>, Jurgen J. Fütterer<sup>b</sup>, Karlijn Rutten<sup>b</sup>, Khrystyna Faryna<sup>a</sup>, Laura Comerma Blesa<sup>v</sup>, Leander van Eekelen<sup>a</sup>, Lee Cooper<sup>w</sup>, Leslie Tessier<sup>a,x</sup>, Ligia Craciun<sup>j</sup>, Mar Navarro-Padilla<sup>b</sup>, Mart van Rijthoven<sup>a</sup>, Maschenka Balkenhol<sup>a,y</sup>, Matthieu J.C.M. Rutten<sup>b,z</sup>, Mattijs Elshot<sup>aa,ab</sup>, Max J. J. de Grauw<sup>b</sup>, Megan Schuurmans<sup>b</sup>, Michiel Simons<sup>a</sup>, Miriam Groeneveld<sup>b</sup>, Mohamed Amgad<sup>w</sup>, Mohammed R. S. Sunoqrot<sup>aa,ab</sup>, Natália Alves<sup>b</sup>, Nefise Uysal<sup>a</sup>, Nikolas Lessmann<sup>b</sup>, Noa Antonissen<sup>b</sup>, Paulo Guilherme de Oliveira Salles<sup>ac</sup>, Paul K. Gerke<sup>b</sup>, Quintin van Lohuizen<sup>i</sup>, Rachel S. van der Post<sup>a</sup>, Robert Jan Kroeze<sup>ad</sup>, Robin Lomans<sup>a</sup>, Shoko Vos<sup>a</sup>, Stefan J. Fransen<sup>i</sup>, Tone F. Bathen<sup>aa,ab</sup>, Valentina Angerilli<sup>a</sup>, Ward Hendrix<sup>b</sup>, Witali Aswolinskiy<sup>a</sup>, Zaigham Saghir<sup>af</sup>, James A. Meakin<sup>b</sup>, Anne Mickan<sup>b</sup>, Thomas Koopman<sup>d,e</sup>, Mathias Prokop<sup>b</sup>, Ewoud J. Smit<sup>b</sup>, Geert Litjens<sup>a,c</sup>, Jeroen van der Laak<sup>a</sup>, Bram van Ginneken<sup>b</sup>, Maarten de Rooij<sup>b</sup>, Henkjan Huisman<sup>b</sup>, Colin Jacobs<sup>b</sup>, Francesco Ciompi<sup>a,†</sup>, Alessa Hering<sup>b,†</sup>

### Affiliations:

- <sup>a</sup> Department of Pathology, Radboud University Medical Center, Nijmegen, The Netherlands  
<sup>b</sup> Department of Medical Imaging, Radboud University Medical Center, Nijmegen, The Netherlands  
<sup>c</sup> Oncode Institute, Utrecht, the Netherlands  
<sup>d</sup> Informatics Institute, Faculty of Science, University of Amsterdam, Amsterdam, The Netherlands  
<sup>e</sup> Departments of Biomedical Engineering and Physics, University Medical Center Amsterdam, Amsterdam, The Netherlands  
<sup>f</sup> Faculty of Medicine, University of Oradea in Oradea, Romania  
<sup>g</sup> Department of Pathology, Herlev-Gentofte Hospital, Herlev, Denmark  
<sup>h</sup> Department of Clinical Medicine, Copenhagen University, Copenhagen, Denmark <sup>i</sup> Department of Radiology, University Medical Center Groningen, Groningen, The Netherlands  
<sup>j</sup> Department of Pathology, Institut Jules Bordet, Université Libre de Bruxelles (ULB), Brussels, Belgium  
<sup>k</sup> Department of Radiology and Nuclear Medicine, Martini Hospital, Groningen, The Netherlands  
<sup>l</sup> University of Groningen, Groningen, Netherlands  
<sup>m</sup> Department of Pathology, Antwerp University Hospital, Edegem, Belgium  
<sup>n</sup> Department of Pathology, AZ Sint-Maarten, Mechelen, Belgium  
<sup>o</sup> Department of Pathology, Herlev and Gentofte Hospital, Herlev, Denmark  
<sup>p</sup> Department of Clinical Medicine, University of Copenhagen, Denmark  
<sup>q</sup> Great Western Hospitals NHS Foundation Trust, Swindon, United Kingdom  
<sup>r</sup> Department of Health & Information Technology, Ziekenhuisgroep Twente, Almelo, The Netherlands  
<sup>s</sup> Department of Radiology, Ziekenhuisgroep Twente, Almelo, The Netherlands  
<sup>t</sup> Department of Radiology and Nuclear Medicine, Rijnstate Hospital, Arnhem, The Netherlands  
<sup>u</sup> Andros Clinics, The Netherlands  
<sup>v</sup> Department of Pathology, Hospital del Mar, Barcelona, Spain  
<sup>w</sup> Department of Pathology, Northwestern University Feinberg School of Medicine, Chicago, IL, United States of America  
<sup>x</sup> Institut du cancer de l'Ouest, University hospital, Angers France  
<sup>y</sup> Department of Pathology, Canisius Wilhelmina Hospital, Nijmegen, the Netherlands  
<sup>z</sup> Department of Radiology, Jeroen Bosch Hospital, 's-Hertogenbosch, The Netherlands  
<sup>aa</sup> Department of Radiology and Nuclear Medicine, St Olavs Hospital, Trondheim University Hospital, Trondheim, Norway  
<sup>ab</sup> Department of Circulation and Medical Imaging, The Norwegian University of Science and Technology – NTNU, Trondheim, Norway  
<sup>ac</sup> Anatomical Pathology Service, Instituto Mário Penna, Belo Horizonte, Brazil  
<sup>ad</sup> Department of Radiology, Sint Maartenskliniek, Nijmegen, The Netherlands  
<sup>af</sup> Department of Medicine, Section of Pulmonary Medicine, Herlev-Gentofte Hospital, Hellerup, Denmark

## 6 Author Contributions

M.S., L.P., F.vd.G., J.S.B., and A.H. wrote the manuscript, F.C. initiated UNICORN, M.S., L.P., F.vd.G., M.D.A., C.G., L.B., J.S.B., J.L., R.A.W., F.C., and A.H. designed the UNICORN framework, M.S., L.P., F.vd.G., M.D.A., C.G., L.B., J.S.B., J.L., and R.A.W. developed the baseline, M.S., L.P.,

F.vd.G., M.D.A., C.G., L.B., J.S.B., J.L., R.A.W., F.C., and A.H. performed UNICORN-specific data preparation and curation and wrote task descriptions, J.A.M., T.K., and A.M. developed new Grand Challenge functionalities for UNICORN, A.M. and C.v.R. provided technical support for Grand Challenge, J.A.M., T.K., A.M., C.v.R., M.G., P.K.G., H.v.Z., and C.I.S.G. developed Grand Challenge, M.St., M.D.A., C.G., L.B., J.S.B., J.L., A.V., A.S., A.L., B.O., C.I.S.G., C.v.R., C.R., D.T., D.L., D.R., D.Y., Di.P., Dr.P., E.I.S.S., E.M.G.T., E.Th.S., G.S., H.v.Z., Ha.H., I.M.E.S., I.D.N., I.S., J.J.T., J.vd.G., J.G., J.V., J.v.S., J.B., J.M.A.S., J.J.I., J.J.F., K.R., K.F., L.C.B., L.v.E., L.C., L.T., L.C., M.N.P., M.v.R., M.B., M.J.C.M.R., M.E., M.J.J.d.G., M.Sc., M.Si., M.G., M.A., M.R.S.S., Na.A., N.U., N.L., No.A., P.G.O.S., P.K.G., Q.v.L., R.S.vd.P., R.J.K., R.L., S.V., S.J.F., T.F.B., V.A., W.H., W.A., Z.S., M.P., E.J.S., G.L., J.vd.L., B.v.G., M.d.R., He.H., C.J., F.C., and A.H. contributed to original challenges or datasets that were reused for UNICORN, M.P., B.v.G., G.L., C.J., E.J.S., M.d.R., H.H., J.vd.L., F.C. and A.H. supervised the mainline Ph.D. candidates, F.C. and A.H. did UNICORN project supervision and management. All authors read and approved the manuscript.

## References

- [1] K. van Leeuwen, M. de Rooij, S. Schalekamp, B. van Ginneken, and M. Rutten. Clinical use of artificial intelligence products for radiology in the Netherlands between 2020 and 2022. *European radiology* 2024 34, 348:354. DOI: 10.1007/s00330-023-09991-5.
- [2] A. Saha, J. S. Bosma, J. J. Twilt, et al. Artificial intelligence and radiologists in prostate cancer detection on MRI (PI-CAI): an international, paired, non-inferiority, confirmatory study. *The Lancet Oncology* 2024 25, 879:887. DOI: 10.1016/S1470-2045(24)00220-1.
- [3] M. van Rijthoven, W. Aswolinskiy, L. Tessier, et al. Tumor-infiltrating lymphocytes in breast cancer through artificial intelligence: biomarker analysis from the results of the TIGER challenge. *medRxiv* 2025. eprint: <https://www.medrxiv.org/content/early/2025/03/03/2025.02.28.25323078.full.pdf>.
- [4] A. A. A. Setio, A. Traverso, T. de Bel, et al. Validation, comparison, and combination of algorithms for automatic detection of pulmonary nodules in computed tomography images: The LUNA16 challenge. *Medical Image Analysis* 2017 42, 1:13. DOI: 10.1016/j.media.2017.06.015.
- [5] T. Chen, S. Kornblith, M. Norouzi, and G. Hinton. A simple framework for contrastive learning of visual representations. *International conference on machine learning*. PmlR. 2020, 1597:1607.
- [6] T. Brown, B. Mann, N. Ryder, et al. Language models are few-shot learners. *Advances in neural information processing systems* 2020 33, 1877:1901.
- [7] J. Devlin, M.-W. Chang, K. Lee, and K. Toutanova. Bert: Pre-training of deep bidirectional transformers for language understanding. *Proceedings of the 2019 conference of the North American chapter of the association for computational linguistics: human language technologies*. Vol. 1. 2019, 4171:4186.
- [8] X. Wang, S. Yang, J. Zhang, et al. Transformer-based unsupervised contrastive learning for histopathological image classification. *Medical image analysis* 2022 81, p. 102559. DOI: 10.1016/j.media.2022.102559.
- [9] A. Filiot, R. Ghermi, A. Olivier, et al. Scaling self-supervised learning for histopathology with masked image modeling. *medRxiv* 2023. DOI: 10.1101/2023.07.21.23292757.
- [10] R. J. Chen, T. Ding, M. Y. Lu, et al. Towards a general-purpose foundation model for computational pathology. *Nature Medicine* 2024 30, 850:862. DOI: 10.1038/s41591-024-02857-3.
- [11] S. Pai, I. Hadzic, D. Bontempi, et al. Vision Foundation Models for Computed Tomography. *arXiv preprint* 2025. DOI: 10.48550/arXiv.2501.09001.
- [12] S. Pai, D. Bontempi, I. Hadzic, et al. Foundation model for cancer imaging biomarkers. *Nature machine intelligence* 2024 6, 354:367. DOI: 10.1038/s42256-024-00807-9.
- [13] J. Jiao, J. Zhou, X. Li, et al. USFM: A universal ultrasound foundation model generalized to tasks and organs towards label efficient image analysis. *Medical Image Analysis* 2024 96, p. 103202. DOI: 10.1016/j.media.2024.103202.
- [14] Z. Wang, Z. Wu, D. Agarwal, and J. Sun. MedCLIP: Contrastive learning from unpaired medical images and text. *Proceedings of the Conference on Empirical Methods in Natural Language Processing. Conference on Empirical Methods in Natural Language Processing*. 2022, p. 3876.

- [15] K. Saab, T. Tu, W.-H. Weng, et al. Capabilities of gemini models in medicine. *arXiv preprint arXiv:2404.18416* 2024.
- [16] T. Tu, S. Azizi, D. Driess, et al. Towards generalist biomedical AI. *N Engl J Med Ai* 2024 1. DOI: 10.1056/AIoa2300138.
- [17] I. E. Hamamci, S. Er, F. Almas, et al. A foundation model utilizing chest CT volumes and radiology reports for supervised-level zero-shot detection of abnormalities. *CoRR* 2024. DOI: <https://arxiv.org/abs/2403.17834v1>.
- [18] L. Blankemeier, J. P. Cohen, A. Kumar, et al. Merlin: A vision language foundation model for 3D computed tomography. *Research Square* 2024. DOI: 10.21203/rs.3.rs-4546309/v1.
- [19] S. Xu, L. Yang, C. Kelly, et al. Elixr: Towards a general purpose x-ray artificial intelligence system through alignment of large language models and radiology vision encoders. *arXiv preprint arXiv:2308.01317* 2023. DOI: 10.48550/arXiv.2308.01317.
- [20] S. Bannur, S. Hyland, Q. Liu, et al. Learning to exploit temporal structure for biomedical vision-language processing. *Proceedings of the IEEE/CVF Conference on Computer Vision and Pattern Recognition*. 2023, 15016:15027.
- [21] W. Ikezogwo, S. Seyfioglu, F. Ghezloo, et al. *Quilt-1m: One million image-text pairs for histopathology*. 2023. arXiv: 2306.11207.
- [22] M. Y. Lu, B. Chen, D. F. Williamson, et al. A visual-language foundation model for computational pathology. *Nature Medicine* 2024 30, 863:874. DOI: 10.1038/s41591-024-02856-4.
- [23] M. Antonelli, A. Reinke, S. Bakas, et al. The medical segmentation decathlon. *Nature communications* 2022 13, p. 4128. DOI: 10.1038/s41467-022-30695-9.
- [24] J. Ma, Y. Zhang, S. Gu, et al. Fast and Low-GPU-memory abdomen CT organ segmentation: The FLARE challenge. *Medical Image Analysis* 2022 82, p. 102616. DOI: 10.1016/j.media.2022.102616.
- [25] Y. Ji, H. Bai, C. Ge, et al. AMOS: A large-scale abdominal multi-organ benchmark for versatile medical image segmentation. *Advances in neural information processing systems* 2022 35, 36722:36732.
- [26] CHAOS Challenge - combined (CT-MR) healthy abdominal organ segmentation. *Medical Image Analysis* 2021 69, 1361:8415. DOI: 10.1016/j.media.2020.101950.
- [27] A. Hering, L. Hansen, T. C. Mok, et al. Learn2Reg: comprehensive multi-task medical image registration challenge, dataset and evaluation in the era of deep learning. *IEEE Transactions on Medical Imaging* 2022 42, 697:712.
- [28] D. Zimmerer, P. M. Full, F. Isensee, et al. Mood 2020: A public benchmark for out-of-distribution detection and localization on medical images. *IEEE transactions on medical imaging* 2022 41, 2728:2738.
- [29] G. Campanella, S. Chen, M. Singh, et al. A clinical benchmark of public self-supervised pathology foundation models. *Nature Communications* 2025 16, p. 3640. DOI: 10.1038/s41467-025-58796-1.
- [30] D. Wang, X. Wang, L. Wang, et al. A real-world dataset and benchmark for foundation model adaptation in medical image classification. *Scientific Data* 2023 10, p. 574. DOI: 10.1038/s41597-023-02460-0.
- [31] kaiko.ai, I. Gatopoulos, N. Känzig, R. Moser, and S. Otálora. eva: Evaluation framework for pathology foundation models. *Medical Imaging with Deep Learning*. 2024. URL: <https://openreview.net/forum?id=FNBQOPj18N>.
- [32] R. Jin, Z. Xu, Y. Zhong, et al. Fairmedfm: fairness benchmarking for medical imaging foundation models. *Advances in Neural Information Processing Systems* 2024 37, 111318:111357.
- [33] E. Beeching, S. Han, N. Lambert, et al. *Open LLM Leaderboard*. [https://huggingface.co/spaces/HuggingFaceH4/open\\_llm\\_leaderboard](https://huggingface.co/spaces/HuggingFaceH4/open_llm_leaderboard). 2023.
- [34] J. S. Bosma, K. Dercksen, L. Bultjes, et al. The DRAGON benchmark for clinical NLP. *npj Digital Medicine* 2025 8, 1:10. DOI: 10.1038/s41746-025-01626-x.
- [35] R. K. Arora, J. Wei, R. S. Hicks, et al. Healthbench: Evaluating large language models towards improved human health. *arXiv preprint arXiv* 2025. DOI: 10.48550/arXiv.2505.08775.

- [36] S. Bedi, H. Cui, M. Fuentes, et al. MedHELM: Holistic Evaluation of Large Language Models for Medical Tasks. *arXiv preprint* 2025. DOI: 10.48550/arXiv.2505.23802.
- [37] J. Meakin, P. K. Gerke, S. Kerkstra, et al. *Grand-Challenge.org*. Version v2023.10. Oct. 25, 2023. DOI: 10.5281/ZENODO.3356819. URL: <https://zenodo.org/doi/10.5281/zenodo.3356819> (visited on 11/23/2023).
- [38] M. D’Amato, R. Weber, J. Lefkes, et al. *The UNICORN Challenge: public few-shots*. Version 7.0. June 17, 2025. DOI: 10.5281/ZENODO.14832502. URL: <https://zenodo.org/doi/10.5281/zenodo.14832502> (visited on 11/07/2025).

# Supplementary Appendix

## Supplemental 1 Tasks

### Supplemental 1.1 Vision – classification

#### **T1: Classifying H&E-stained prostate biopsies into ISUP scores**

This task involves classifying prostate biopsies as either benign or into one of the five International Society of Urological Pathology (ISUP) grade groups. The dataset includes a total of 308 H&E-stained whole-slide images (WSI) from prostate cancer patients in screening programs and hospital evaluations. Data was collected from two cohorts: 195 whole-slide images from Radboudumc (2012–2017) for the validation set and for the test set, 113 whole-slide images from six hospitals, the Rennes University Hospital (France), Radboudumc (Netherlands), Institute of Pathology and Molecular Immunology of the University of Porto (Portugal), Memorial Hospitals Istanbul (Turkey), Foch Hospital (France), and Isala Zwolle (Netherlands), collected as part of the Evaluating AI-based Gleason grading in-the-wild study [1] to ensure a diverse and representative set of prostate biopsy slides from routine clinical practice.

The first cohort is sampled from the test set of the PANDA challenge [2]<sup>3</sup>. The reference standard was established through a three-round grading procedure involving three expert uropathologists, following the ISUP 2014 guidelines. In the first round, all cases were graded independently. If at least two pathologists agreed on the ISUP grade group, the majority vote was accepted, including cases where the disagreement was limited to the Gleason pattern order (e.g., 4+5 vs. 5+4) or minor differences in score interpretation. Cases with a disagreement on malignancy were always flagged for further review. In the second round, cases without consensus were regraded by the outlier pathologist, i.e., the one whose score deviated most from the other two. During this step, the anonymous scores from the other two pathologists were made available to aid re-evaluation. In the third round, any remaining cases without agreement were reviewed in a consensus meeting. For the second cohort, a single representative biopsy per case was selected by a pathology resident under the supervision of a uropathologist. A reader study involving 10 pathologists established the reference standard. For each case, the final label was assigned through a two-step process: first, the sample was categorized as benign or cancerous based on the 10 grades. If deemed cancerous, a majority vote among the cancer grades determined the final label. In case of ties, the highest Gleason grade group was assigned.

Data was obtained in various formats, but is provided in the benchmark as multi-resolution .tif files with a starting resolution of 0.50 microns per pixel, along with a binary tissue mask (0=background, 1=tissue). For each case, the expected prediction is a single integer ranging from 0 to 5. Task performance is assessed using Cohen’s quadratic weighted kappa.

#### **T2: Classifying lung nodule malignancy in CT**

The main goal of this task is to predict a nodule malignancy probability for a nodule candidate, indicating either a low or high risk of malignancy. The test data is from the Danish Lung Cancer Screening Trial (DLCST)[3], which includes low-dose CT thorax-abdomen scans from between 2004 and 2010, containing 533 nodules from 533 participants. Participants aged 50–70 years at the time of inclusion and with a minimum of 20 pack-years of smoking were included. Each case contains one nodule block of 128×128×64 voxels from the low-dose CT thorax-abdomen scans provided in the MHA file format. No additional preprocessing was performed. The first occurrence of a malignant nodule for each cancer was selected, and then one malignant nodule per participant was randomly selected and annotated. A positive cancer case refers to a scan with at least one malignant nodule, confirmed by histopathological examination. Benign nodules are only provided from non-lung cancer scans with at least 2 years of imaging follow-up. The nodule locations were annotated as center coordinates by two experienced chest radiologists. The scans were acquired with a 16-slice Philips Mx 8000, and scans were taken with the patient supine after full inspiration using a low-dose technique (120 kV and 40 mA).

For each case, the prediction is expected to be a continuous model probability score between 0 and 1. The task will be assessed using the area under the receiver operating characteristic curve (AUROC) to evaluate performance in distinguishing between benign and malignant nodules.

This dataset is similar to a subset of the testing dataset used in the LUNA25 challenge [4]<sup>4</sup>, with key differences being that the UNICORN task 2 testing set contains nodules of all sizes, not only of the

---

<sup>3</sup><https://panda.grand-challenge.org/>

<sup>4</sup><https://luna25.grand-challenge.org/>

indeterminate size range, and that it is not cancer-enriched.

#### **T4: Predicting slide-level tumor proportion score in NSCLC IHC-stained WSI**

The goal in this task is to predict the tumor proportion score (TPS) in PD-L1 immunohistochemistry-stained whole-slide images from non-small cell lung cancer (NSCLC). The dataset includes a total of 639 WSIs from 505 lung cancer patients from Radboudumc, including biopsies from both primary lung tumors and metastatic sites.

Each individual case is provided on the platform as a .tif file with a resolution of 0.50 microns per pixel, accompanied by a binary tissue mask (0=background, 1=tissue). Positive control tissue was excluded from the WSIs, as its sole purpose is to verify the success of the immunohistochemical staining procedure. The reference standard for each case is a binned TPS value, extracted from pathology reports and based on visual estimates by experienced lung pathologists. In clinical settings, these estimates are typically categorized into three bins: less than one percent, one percent to less than fifty percent, and fifty percent or greater. The expected prediction for each case is a single integer (0,1,2) reflecting one of the 3 bins. Performance is evaluated using Cohen’s quadratic weighted kappa between predicted and reference TPS bins.

### **Supplemental 1.2 Vision – regression**

#### **T3: Predicting the time to biochemical recurrence in H&E-stained prostatectomies**

This task aims to estimate the risk of biochemical recurrence in prostate cancer patients after a radical prostatectomy. Biochemical recurrence is defined as PSA > 0.2 ng/mL on two or more occasions after having previously reached an undetectable level post-prostatectomy. The dataset includes H&E-stained whole prostatectomy slides for 570 patients, with follow-up for prostate-specific antigen (PSA) blood measurements. Data was collected from two cohorts: 149 patients from Radboudumc (Netherlands), and 421 patients from Instituto Mário Penna (Brazil).

Each case is provided as multi-resolution .tif files, with a starting resolution of 0.50 microns per pixel along with a binary tissue mask (0=background, 1=tissue). The label for each case indicates whether biochemical recurrence occurred (0=no biochemical recurrence, 1=biochemical recurrence), and the time in years to recurrence or the last follow-up. No human annotators were involved, as the biochemical recurrence is used as the primary endpoint.

For each case the prediction should be a continuous time estimate (float) for the time to biochemical recurrence (in years). Performance is evaluated using the censored concordance index.

Task 3 is adapted from the LEOPARD challenge [5]<sup>5</sup>. Unlike the LEOPARD challenge, which relied on local training with large datasets, this task follows a few-shot learning paradigm, with training performed on-platform.

### **Supplemental 1.3 Vision – detection**

#### **T5: Cell detection of signet ring cells in H&E-stained WSI of gastric cancer**

This task aims to detect signet ring cells in H&E-stained whole-slide images of gastric cancer. The dataset includes 478 regions of interest (ROIs) extracted from 259 WSIs of 35 patients from Radboudumc, all scanned using the same scanner. Each ROI is considered one case and is saved as an individual .tif file at a starting resolution of 0.5 microns per pixel.

ROIs with diffuse gastric cancer tumor lesions, including pre-invasive lesions, were selected by a resident pathologist. All signet ring cells were annotated as (x,y) coordinates by student annotators, with all annotations subsequently verified by a pathologist with expertise in gastric cancer.

The expected prediction for each case consists of predicted (x,y) coordinates of detected signet ring cells within the case. Performance is evaluated using the F1 score. If multiple predicted points hit one ground truth point, this is counted as 1 true positive and 0 false negatives. If one predicted point is a hit for N ground truth points, this is counted as 1 true positive and N-1 false negatives.

#### **T6: Detecting clinically significant cancer in prostate MRI exams**

The objective in this task is to perform 3D detection of clinically significant prostate cancer lesions with an ISUP score  $\geq 2$ , using biparametric MRI scans. The patient population includes individuals

---

<sup>5</sup><https://leopard.grand-challenge.org/>

suspected of harboring clinically significant prostate cancer based on elevated PSA levels or abnormal DRE findings, with no prior treatment or history of ISUP  $\geq 2$  findings. Each case within the benchmark comprises axial T2-weighted (T2W) scans, axial high b-value ( $\geq 1000s/mm^2$ ) diffusion-weighted imaging (DWI), and axial apparent diffusion coefficient (ADC) maps. Test data consists of 400 cases and includes all three imaging sequences (axial T2W, DWI, and ADC). Data was collected from Radboudumc, Ziekenhuisgroep Twente, Prostaat Centrum Noord-Nederland, and St. Olav’s Hospital in Norway, using Siemens or Philips scanners. The reference standard for validation and testing incorporates histopathological evidence (ISUP  $\geq 2$  for positives, ISUP  $\leq 1$  or MRI PI-RADS  $\leq 2$  with  $\geq 3$  years follow-up for negatives). Annotations for cases were performed by trained investigators under expert supervision. These annotations were based on MRI exams, diagnostic reports, and pathology specimens, undergoing quality control and independent cross-checking at the coordinating medical center. The evaluation metric is the average of the area under the receiver operating characteristic curve (AUROC) and the area under the precision-recall curve (AP). Task 6 is adapted from the PI-CAI challenge [6]<sup>6</sup>. Validation and test datasets mirror those used in PI-CAI, with the test dataset mirroring the reader study subset, but omitting clinical parameters and coronal/sagittal T2 images.

### **T7: Detecting lung nodules in thoracic CT**

The main goal of this task is to accurately detect pulmonary nodules in both clinical routine chest CT scans. The test cohort of 83 patients includes clinical scans collected in the period of 2018-2020 at Radboudumc. The test set is sourced from one of the hospitals in a previous study [7], however, from 100 patients the test set was filtered to 83. We filtered scans for which the majority (3/5) of the radiologists agreed on the presence of the nodule, to create a test set with a reliable reference standard. Patients include those receiving thorax CTs as part of clinical care, who are above 18 years old, and in whom a nodule was incidentally detected. Both contrast-enhanced and non-contrast CT scans are included. Data acquisition involved scanners from various manufacturers, including Philips, Siemens, and Canon models. The dataset was annotated by a panel of five experienced thoracic radiologists using specialized in-house software to identify and measure intrapulmonary nodules and generate coordinates. Each case contains one CT volume provided in .mha format (512 x 512 px), with no pre-processing applied. The model predictions are evaluated using sensitivity and false positive rate per scan. To be a true positive, the lesion candidate should be located within a distance  $R$  of the nodule center, where  $R$  is set to the equivalent diameter of the nodule divided by 2. Lesion candidates that do not correspond to any nodule are considered false positives. Lesion candidates corresponding to irrelevant findings are ignored during the evaluation and are not considered either false positives or true positives. Performance is assessed in the same way as the LUNA16 challenge, using a Free Receiver Operating Characteristic (FROC) analysis and the competition performance metric (CPM) is defined as the average sensitivity at 7 predefined false positive rates: 1/8, 1/4, 1/2, 1, 2, 4, and 8 false positives per scan. If none of the candidates result in a true positive, a score of 0 for the CPM will be assigned. Task 7 is inspired by the LUNA16 challenge [8]<sup>7</sup>.

### **T8: Cell detection of mitotic figures in breast cancer H&E-stained WSIs**

The goal of this task is to accurately detect mitotic figures in H&E-stained whole-slide images of triple-negative breast cancer. The dataset includes 400 regions of interest (ROIs) extracted from 11 whole-slide images from patients from Radboudumc. Each ROI is considered one case and extracted and saved as an individual .tif file at a resolution of 0.25 microns per pixel. All ROIs are selected using random probability sampling, where ROIs with higher mitotic count are more likely to be sampled. Annotations of all mitotic figures are provided as the (x, y) coordinates within the case. Each mitotic figure has been validated using a PHH3 marker, clearly highlighting the mitotic cells, on an immunohistochemistry-stained image. The clearly marked cells by the PHH3 marker were used for registration to the corresponding H&E-stained image.

The expected prediction for each case should be all the predicted (x,y) coordinates of the mitotic figures. The performance is evaluated using the F1-score. If multiple predicted points hit one ground truth point, this is counted as 1 true positive and 0 false negatives. If one predicted point is a hit for N ground truth points, this is counted as 1 true positive and N-1 false negatives.

<sup>6</sup><https://pi-cai.grand-challenge.org/>

<sup>7</sup><https://luna16.grand-challenge.org/>

## Supplemental 1.4 Vision – segmentation

### T9: Segmenting ROIs in breast cancer H&E-stained WSIs

Within this task, the objective is to segment breast tissue into tumor, stroma, and other in H&E-stained whole-slide images. The dataset includes 33 regions of interest (ROIs) from 11 whole-slide images from Radboudumc and the Jules Bordet Institute. Each case is an ROI of approximately 500x500 microns extracted and saved as individual .tif files at a resolution of 0.50 microns per pixel. Each ROI was annotated by five board-certified breast pathologists from the tumor-infiltrating lymphocyte working group. All data was adopted from the TIGER challenge [9]<sup>8</sup>, however, only a subset of sequestered data was used in the form of ROIs instead of WSIs.

The prediction for each case should be a 2D array with pixel-level segmentation of four classes (0=background, 1=tumor, 2=stroma, 3=other). Performance is assessed using the Dice coefficient.

### T10: Segmenting lesions within ROIs in CT

This task focuses on segmenting lesions within ROIs in chest-abdomen-pelvis CT examinations. The goal of this task is to segment 3D masks of lesions in CT scans. The dataset includes CT sub-images of lesions from 725 cases (46.5% female) sourced from Radboudumc and Jeroen Bosch Ziekenhuis in the Netherlands. Each case comprises a volume of interest (VOIs) of  $256 \times 256 \times 128$  voxels. Each VOI centers on a lesion voxel to simulate a radiologist’s click. Where necessary, volumes were padded with the minimum intensity value of the VOI minus one. Each VOI contains a single annotated lesion. Three annotators independently annotated each lesion in 3D, and the final mask was determined by majority vote. This mask was reviewed and corrected where necessary by an experienced radiologist. Segmentation performance (SP) is measured using the Sørensen-Dice coefficient. Additional metrics include symmetric mean absolute percentage error for long- and short-axis measurements (LAE and SAE). The final composite score is computed as:

$$CS = 0.888 \cdot SP + 0.056 \cdot LAE + 0.056 \cdot SAE$$

This test set was previously used in the ULS challenge [10]<sup>9</sup>. The evaluation simplifies the original challenge evaluation by omitting the robustness score.

### T11: Segmenting three anatomical structures in lumbar spine MRI

The goal of this task is to segment vertebrae, intervertebral discs, and the spinal canal using lumbar MRI scans. The data includes MRI studies of patients with a history of low back pain, retrospectively collected from four Dutch hospitals in the Netherlands: one university medical center, two regional hospitals, and one orthopedic hospital. The data was acquired between January 2019 and March 2022 and includes 97 MRI series from 39 patients (62% female). Each case is one patient examination that consists of up to three sagittal MRI series, which are either T1-weighted or T2-weighted (regular resolution, or high resolution generated using a SPACE sequence). The voxel size of these sequences ranges from  $0.90 \times 0.47 \times 0.47$  mm to  $9.63 \times 1.06 \times 1.23$  mm. All visible vertebrae (excluding the sacrum), intervertebral discs, and the spinal canal were manually annotated. The annotations were performed by a medical trainee who was trained and supervised by both a medical imaging expert and an experienced musculoskeletal radiologist. The segmentation performance is evaluated using the Dice coefficient measured in 3D. Dice scores are computed for each individual anatomical structure (vertebrae, intervertebral discs, and the spinal canal). Instance-wise scores are then averaged to obtain an overall Dice score.

This test set was previously used in the SPIDER challenge [11]<sup>10</sup>.

## Supplemental 1.5 Language – classification

The language tasks (tasks 12 to 19) are derived from tasks in the DRAGON challenge [12]. For some tasks, the evaluation data is exactly the same as in the DRAGON challenge, while for others, adaptations have been made to align better with generative LLMs, as detailed below. For each task, 32-48 few-shot examples are provided to facilitate in-context learning. All reports were anonymized using the Hide-in-plain-sight (HIPS) [13] algorithm to remove sensitive patient information. Apart from anonymization, no data preprocessing was performed for any of these tasks.

---

<sup>8</sup><https://tiger.grand-challenge.org/>

<sup>9</sup><https://uls23.grand-challenge.org/>

<sup>10</sup><https://spider.grand-challenge.org/>

### **T12: Predicting histopathology sample origin**

The objective in this task is to predict from which organ the material was taken (lung, lymph node, bronchus, liver, brain, bone, or other), as described in the Dutch pathology report. The challenge cohort includes patients suspected of having non-small cell lung cancer between January 1, 2016, and December 31, 2022. The same test and validation sets were used as in Task06 from the DRAGON challenge [12]. For adaptation, 48 few-shot examples were sampled from the training data, without overlap between the validation and test phases, resulting in a total of 608 Dutch pathology reports being included, all originating from Radboudumc. The labels were assigned by trained student assistants based on manual review of the reports. The labels for this task are categorical and the frequency of the labels is unbalanced. The labels are not ordinal. Therefore, model performance is assessed using the unweighted Cohen’s Kappa.

### **T13: Classifying pulmonary nodule presence**

The objective in this task is to determine whether a pulmonary nodule is described in the radiology report or not. Chest CT reports from two Dutch hospitals, acquired between 1 January 2008 and 31 December 2019 from Radboudumc and Jeroen Bosch Ziekenhuis were used [14]. The same test and validation sets were used as in Task07 from the DRAGON challenge [12]. For adaptation, 48 few-shot examples were sampled from the training data, without overlap between the validation and test phases, resulting in a total of 596 Dutch reports being used from 596 unique patients. The dataset reflects real-world class distributions. The test reports were annotated by a radiologist with 26 years of experience. Each report received a binary label indicating the presence or absence of pulmonary nodules. The area under the receiver operating characteristic curve is used to evaluate model performance.

### **T14: Classifying kidney abnormality**

The objective in this task is to identify the presence of significant kidney abnormalities based on the radiology report. The same test and validation sets were used as in Task03 from the DRAGON challenge [12]. For adaptation, 48 few-shot examples were sampled from the training data, without overlap between the validation and test phases, resulting in a total of 404 Dutch radiology reports collected from patients who underwent abdominal CT scans at Radboudumc. Reports were manually analyzed and labeled as either “normal” or “abnormal” by a native Dutch-speaking PhD candidate. Abnormalities include renal cell carcinoma, angiomyolipoma, cysts, kidney stones, conjoined kidneys, cases with partial or full nephrectomy, and several other rare abnormalities. Evaluation is performed using the area under the receiver operating characteristic curve.

### **T15: Predicting hip Kellgren-Lawrence score**

The objective in this task is to classify the radiology report by the Hip Kellgren-Lawrence score for hip osteoarthritis per hip joint, ranging from 0 to 4 with 0 (no osteoarthritis), 1 (doubtful osteoarthritis), 2 (minimal osteoarthritis), 3 (moderate osteoarthritis), and 4 (severe osteoarthritis), or indicate the hip has a prosthesis, or the scoring is not applicable to that hip. The test set is a subset of 108 cases from the original test set from Task018 in the DRAGON challenge [12], the validation set is a subset of 100 cases from the original validation set, and for adaptation, 32 few-shot examples were sampled from the original testing data, without overlap between the validation and test phases resulting in a total of 272 Dutch radiology reports for hip osteoarthritis collected at Radboudumc. Reports were manually annotated by a trained investigator, with difficult cases being reviewed by a radiologist. The labels in the dataset are imbalanced, and while the Kellgren-Lawrence score is ordinal, the additional categories are not. Performance is assessed by pooling the predictions for the left and right hip, and calculating the unweighted Cohen’s Kappa for the combined predictions.

### **T16: Classifying colon histopathology diagnosis**

The objective in this task is to predict whether the specimen was obtained from 1) biopsy or polypectomy, and whether the pathologist rated the specimen as 2) cancer, 3) high-grade dysplasia (hgd), 4) hyperplastic polyps, 5) low-grade dysplasia (lgd), 6) non-informative (ni), or 7) serrated polyps. Each of these seven properties is binary, and multiple can be present per block. Each report conclusion was annotated by native Dutch data analysts under the supervision of two gastrointestinal pathologists. The test set is a subset of 500 cases from the original test set in Task015 from the DRAGON challenge [12]

with sampling strategy to ensure at least 20 positive cases per label, the validation set is a subset of 250 cases from the original validation set with the same sampling strategy, and for adaptation, 48 few-shot examples were sampled from the original training data, without overlap between the validation and test phases and with at least three positive cases per label, resulting in 846 Dutch pathology reports from patients diagnosed with histopathological conditions of the colon, from biopsies performed between January 1, 2000, and December 31, 2009, at Radboudumc. For patients with multiple visits during this time frame, only the first visit was included. The model’s output is expected as a JSON file, containing per case the labels for all eight characteristics. Model performance is evaluated by calculating the area under the receiver operating characteristic curve (AUROC) for each class separately. The overall performance of the model is defined as the average of the AUROC values across all classes.

## Supplemental 1.6 Language – regression

### T17: Predicting lesion size measurements

The objective in this task is to extract the size of three types of lesions which are presented in the report. The lesions to be extracted were offered in the preamble of each report. Data is sourced from three tasks of the DRAGON challenge [12]: pulmonary nodules, RECIST target lesions, and pancreatic ductal adenocarcinomas (PDAC), representing real-world cases of diagnostic procedures. This is a combined subset of Task022, Task023 and Task024 of the DRAGON challenge [12] cohort, using a total of 636 reports. The sequestered test set includes 298 cases distributed across these cohorts: 32 cases to extract the pulmonary nodule size, 119 cases to extract RECIST lesion sizes, and 147 cases to extract the PDAC size. Annotations were manually created by trained investigators or radiologists, ensuring accurate lesion size measurements. Each dataset has specific prediction objectives, such as determining the largest diameter, short axis, or longest axis of lesions, depending on the type of lesion described in the radiology report. Both the report text and the annotations are provided for the few shot cases in a JSON file. Lesion size ranges vary by cohort, with pulmonary nodules measuring between 1–30 mm, RECIST lesions between 4–166 mm, and PDAC diameters between 6–130 mm, as determined by the development data (values in the test set are sequestered), with most values falling within specific diagnostic ranges. Evaluation uses the Robust Symmetric Mean Absolute Percentage Error Score (RSMAPES) with a 4 mm tolerance to ensure diagnostically relevant evaluation.

### T18: Predicting prostate volume, PSA, and PSA density

The objective in this task is to predict the prostate volume, prostate specific antigen (PSA) level, and the PSA density, based on the radiology report. This task was derived from Task019, Task020, and Task021 the DRAGON challenge [12] cohort. Dutch prostate MRI reports were collected from University Medical Center Groningen, Antoni van Leeuwenhoek Ziekenhuis, and Radboudumc. The combined dataset includes 846 cases. Labels were manually annotated by trained investigators and consist of three continuous variables. The prostate volume ranges from 4.0 to 470 cm<sup>3</sup>, with 95% of values between 24 and 181 cm<sup>3</sup>, as determined based on the original task’s development data. The PSA level ranges from 0 to 870 ng/mL, with 95% of values between 2 and 35 ng/mL, as determined based on the original task’s development data. The PSA density ranges from 0 to 171 ng/mL<sup>2</sup>, with 95% of values between 0.03 and 0.6 ng/mL<sup>2</sup>, as determined based on the original task’s development data. Performance for this task is measured using the average of the RSMAPES metric [12] per clinical variable, with epsilon thresholds set at 4 cm<sup>3</sup> for prostate volume, 0.4 ng/mL for PSA level, and 0.04 ng/mL<sup>2</sup> for PSA density. Task 18 is derived from Task019 (prostate volume extraction), Task020 (prostate specific antigen extraction), and Task021 (prostate specific antigen density extraction) of the DRAGON Challenge [12].

## Supplemental 1.7 Language – named entity recognition

### T19: Anonymizing report

The objective in this task is to identify and tag personally identifiable information (PII) within reports, including dates, personal identifiers, report identifiers, locations, clinical trial names, times, and ages. Pathology and radiology reports were sourced from two hospitals (Radboudumc, Antoni van Leeuwenhoek Ziekenhuis) as part of Task025 of the DRAGON challenge [12]. The test set is a subset of 400 cases from the original test set in the DRAGON challenge [12], the validation set is a subset of 200 cases from the original validation set, and for adaptation, 48 few-shot examples were sampled from the original training data, without overlap between the validation and test phases, resulting in a total of 696

cases being included. The reports were annotated semi-automatically by processing the reports with a tool developed in-house (i.e., a rule-based system) and were manually verified and corrected by one of three trained investigators. Performance is assessed using the blended redaction F1 score. This metric combines a strict character-level F1 score checking the correct tag type with a binary character-level F1 score determining whether the span was redacted at all. These values are weighted 0.7 and 0.3 in the final score, respectively.

## **Supplemental 1.8 Vision-language – caption generation**

### **T20: Generating caption from WSI**

This task involves generating a caption for each case that encapsulates the relevant clinical information, such as tissue type and diagnosis, from the whole-slide image (WSI) of colon and cervix biopsies and polyps. The dataset consists of 392 WSI-report pairs from 361 unique patients derived from the ExaMode project, where each case is a WSI linked to its corresponding Dutch pathology reports. The ground truth consists of the conclusion section from the original Dutch pathology report associated with each WSI, which captures the pathologist’s final diagnostic interpretation.

The dataset includes 202 colon cases and 190 cervix cases. To ensure diagnostic diversity and mitigate class imbalance, cases were sampled to evenly represent clinically relevant categories based on standardized protocols for cervix and colon biopsies. For cases with multiple co-occurring diagnoses (e.g., CIN3 with carcinoma), the most clinically severe label guided inclusion.

Each case is provided in the benchmark as .tif WSI, along with its corresponding tissue mask and task description. The algorithms are expected to analyze the WSI, identify key features such as tissue type, cellular morphology, and pathological findings, and produce a clear, clinically meaningful Dutch textual conclusion per case. Performance is evaluated as the average of five metrics: BLEU-4, ROUGE-L, CIDEr, METEOR, and BERTScore.

## **Supplemental 2 Challenge Phases**

To support comprehensive benchmarking, the UNICORN Challenge was arranged in sequential phases, each with specific goals and evaluation criteria.

### **Supplemental 2.1 Off-Platform Development Phase**

Given the limited number of permitted on-platform submissions, strong local development was essential for identifying promising approaches before on-platform evaluation. In the off-platform development phase, users could freely develop and validate their models and aggregation strategies outside the Grand Challenge platform. To support this, we publicly released example datasets for each task, typically sourced from public data and reformatted to match the format and structure of the sequestered data in the on-platform check, validation, and test phases [15]. The examples supported local solution development while ensuring compatibility with the platform’s inputs and outputs. References to existing public datasets were also provided to facilitate further local experimentation, as provided in Table S1.

### **Supplemental 2.2 Check phase**

The check phase was designed to verify that submission pipelines execute correctly on the platform, identify potential issues, and help teams become familiar with the platform’s submission process. Submissions in this phase did not contribute towards the final leaderboard, as the results were not always reflective of model performance because only a handful of cases were used. For this phase, a limited but carefully curated set of few-shot and evaluation cases was selected, including potential edge cases such as extremely large or unusually small images, which are most likely to trigger errors or timeouts. Passing the check phase was a prerequisite for submitting to the corresponding validation or test phase. This requirement contributed to only permitting robust and well-integrated pipelines to progress to later stages, reducing the risk of runtime failures during validation and test evaluations. In addition, users had access to the log file on the platform and could submit an unlimited number of times to the Check Phase, hence conserving their submissions on the validation phase for algorithm improvements rather than debugging. By being able to debug their errors early in the challenge, we were able to save compute costs, as opposed to users discovering errors only in the validation and test phase, which have large numbers of cases.

### Supplemental 2.3 Validation phase

The validation phase was designed to help users assess their model and compare their performance with other teams. Compared to the check phase, more extensive datasets were used, drawn from private sources that either matched or closely resembled the distribution of the final test sets. None of the validation benchmark data was publicly available.

Each task had its own individual validation leaderboard, supporting users in evaluating performance in isolation. To encourage the development of generalizable solutions, combined leaderboards were available, aggregating performance across related tasks based on domain and modality. Four combined leaderboard types were defined: pathology-vision tasks, radiology-vision tasks, language tasks, and an *all-tasks* leaderboard. The all-tasks leaderboard spanned all 20 tasks of the challenge and served as the global benchmark.

To balance evaluation frequency with computational constraints, each team was allowed a maximum of six successful validation submissions per task: three per task-specific leaderboard, two per domain/modality-based combined leaderboard, and one to the all-tasks leaderboard. All successful validation submissions were displayed on their respective leaderboards, allowing users to benchmark their progress and use this feedback to guide algorithm development ahead of the final test phase.

### Supplemental 2.4 Test phase

During the test phase, algorithms were evaluated on sequestered test sets. The primary goal of the challenge was to benchmark the generalizability of foundation models across diverse tasks, rather than optimizing for individual tasks in isolation. Therefore, only combined leaderboards were set up, as described in Supplemental 2.3.

Teams could submit to a test leaderboard only once, and could submit either to the all-tasks or to the combined leaderboards, but not both. If they chose to submit to the all-tasks, their results were automatically considered for ranking within the corresponding combined leaderboards when determining challenge winners.

Overall model performance was summarized via the “UNICORN Score” introduced in Section 3.1.

Final rankings were based on aggregated normalized performance metrics across all tasks in each respective combined leaderboard, providing a comprehensive assessment of each model’s robustness and adaptability. For the overall test leaderboard, the final ranking score is given by Equation 3.

$$\begin{aligned} S_{UNICORN,all} &= \frac{1}{20} \sum_{i=1}^{20} \frac{S_i - S_{majority}}{1 - S_{majority}} \\ &= \frac{1}{20} \left( S_1 + \frac{S_2 - 0.5}{0.5} + \frac{S_3 - 0.5}{0.5} + S_4 + S_5 + \frac{S_6 - 0.25}{0.75} + S_7 + S_8 \right. \\ &\quad \left. + \frac{S_9 - 0.2548}{0.7452} + S_{10} + S_{11} + S_{12} + \frac{S_{13} - 0.5}{0.5} + \frac{S_{14} - 0.5}{0.5} + S_{15} \right. \\ &\quad \left. + \frac{S_{16} - 0.5}{0.5} + \frac{S_{17} - 0.7580}{0.2420} + \frac{S_{18} - 0.7668}{0.2332} + S_{19} + S_{20} \right) \end{aligned} \quad (3)$$

### Supplemental 3 Example code

To help users get started, a set of open-source repositories covering various aspects of the challenge was released. These resources serve both as functional templates and as reference implementations to support local development and on-platform submissions.

The *minimal working template*<sup>11</sup> includes only the essential code for preprocessing inputs and formatting outputs according to the platform’s specifications. This template does not perform actual model inference; instead, it uses intensity statistics as stand-in features, allowing users to verify integration and understand the expected input/output structure.

The *full reference solution* provides a baseline solution<sup>12</sup> using publicly available models. The repository includes end-to-end logic for all supported tasks, including data preprocessing and feature extraction. This implementation, based on publicly available models and equipped with lightweight adaptors, successfully executes across all tasks and produces a UNICORN score of 0.378.

<sup>11</sup>[https://github.com/DIAGNijmegen/unicorn\\_baseline\\_template](https://github.com/DIAGNijmegen/unicorn_baseline_template)

<sup>12</sup>[https://github.com/DIAGNijmegen/unicorn\\_baseline](https://github.com/DIAGNijmegen/unicorn_baseline)

Finally, a repository with *adaptor strategies and evaluation logic*<sup>13</sup> contains adaptor implementations for the vision tasks and the evaluation code, making all task-specific metric computations publicly available. Benchmark users were encouraged to contribute new adaptors via pull requests.

## Supplemental 4 Tables

Table S1: Public Datasets for the Development Phase

Task	Dataset	License	Public Links	Publication
1	PANDA	CC BY-NC-SA 4.0	<a href="https://www.kaggle.com/c/prostate-cancer-grade-assessment/data">https://www.kaggle.com/c/prostate-cancer-grade-assessment/data</a>	[2]
2	LUNA25	CC-BY CC-BY-NC	<a href="https://zenodo.org/records/14223624">https://zenodo.org/records/14223624</a> <a href="https://zenodo.org/records/14673658">https://zenodo.org/records/14673658</a>	[16]
3	LEOPARD	CC BY-NC-SA	<a href="https://leopard.grand-challenge.org/">https://leopard.grand-challenge.org/</a>	[5]
4	LUNG_18-193	CC BY 4.0	<a href="https://www.synapse.org/Synapse:syn26722626">https://www.synapse.org/Synapse:syn26722626</a>	[17]
5	DigestPath	CC BY 4.0	<a href="https://digestpath2019.grand-challenge.org/">https://digestpath2019.grand-challenge.org/</a>	[18]
6	PI-CAI	CC BY 4.0	<a href="https://zenodo.org/record/6624726">https://zenodo.org/record/6624726</a>	[6]
7	LUNA16	CC BY 4.0	<a href="https://zenodo.org/records/3723295">https://zenodo.org/records/3723295</a> <a href="https://zenodo.org/records/4121926">https://zenodo.org/records/4121926</a>	[8] [19]
8	MIDOG	CC BY 4.0	<a href="https://zenodo.org/records/4643381">https://zenodo.org/records/4643381</a>	[20]
9	TIGER	CC BY-NC 4.0	<a href="https://zenodo.org/records/6014422">https://zenodo.org/records/6014422</a> <a href="https://doi.org/10.5281/zenodo.6014420">https://doi.org/10.5281/zenodo.6014420</a>	[9]
10	ULS23	CC BY-NC-SA 4.0	<a href="https://zenodo.org/records/10035161">https://zenodo.org/records/10035161</a> <a href="https://zenodo.org/records/10050960">https://zenodo.org/records/10050960</a> <a href="https://zenodo.org/records/10054306">https://zenodo.org/records/10054306</a> <a href="https://zenodo.org/records/10054702">https://zenodo.org/records/10054702</a> <a href="https://zenodo.org/records/10057471">https://zenodo.org/records/10057471</a> <a href="https://zenodo.org/records/10056235">https://zenodo.org/records/10056235</a>	[10]
11	SPIDER	CC BY 4.0	<a href="https://zenodo.org/records/10159290">https://zenodo.org/records/10159290</a>	[11]
12	DRAGON	CC BY-NC-SA 4.0	Task 13 of DRAGON: <a href="https://github.com/DIAGNijmegen/dragon_sample_reports/">https://github.com/DIAGNijmegen/dragon_sample_reports/</a>	[12]
13	DRAGON	CC BY-NC-SA 4.0	Task 2 of DRAGON: <a href="https://github.com/DIAGNijmegen/dragon_sample_reports/">https://github.com/DIAGNijmegen/dragon_sample_reports/</a>	[12]
14	DRAGON	CC BY-NC-SA 4.0	Task 3 of DRAGON: <a href="https://github.com/DIAGNijmegen/dragon_sample_reports/">https://github.com/DIAGNijmegen/dragon_sample_reports/</a>	[12]
15	DRAGON	CC BY-NC-SA 4.0	Task 18 of DRAGON: <a href="https://github.com/DIAGNijmegen/dragon_sample_reports/">https://github.com/DIAGNijmegen/dragon_sample_reports/</a>	[12]
16	DRAGON	CC BY-NC-SA 4.0	Task 15 of DRAGON: <a href="https://github.com/DIAGNijmegen/dragon_sample_reports/">https://github.com/DIAGNijmegen/dragon_sample_reports/</a>	[12]
17	DRAGON	CC BY-NC-SA 4.0	Tasks 22, 23, 24 of DRAGON: <a href="https://github.com/DIAGNijmegen/dragon_sample_reports/">https://github.com/DIAGNijmegen/dragon_sample_reports/</a>	[12]
18	DRAGON	CC BY-NC-SA 4.0	Tasks 19, 20, 21 of DRAGON: <a href="https://github.com/DIAGNijmegen/dragon_sample_reports/">https://github.com/DIAGNijmegen/dragon_sample_reports/</a>	[12]
19	DRAGON	CC BY-NC-SA 4.0	Task 25 of DRAGON: <a href="https://github.com/DIAGNijmegen/dragon_sample_reports/">https://github.com/DIAGNijmegen/dragon_sample_reports/</a>	[12]
20	WsiCaption	N/A	<a href="https://github.com/cpystan/Wsi-Caption">https://github.com/cpystan/Wsi-Caption</a>	[21]

## References

- [1] K. Faryna, L. Tessier, J. Retamero, et al. Evaluation of Artificial Intelligence-Based Gleason Grading Algorithms “in the Wild”. *Modern Pathology* 2024 37, p. 100563. ISSN: 0893-3952. DOI: 10.1016/j.modpat.2024.100563.

<sup>13</sup>[https://github.com/DIAGNijmegen/unicorn\\_eval](https://github.com/DIAGNijmegen/unicorn_eval)

- [2] W. Bulten, K. Kartasalo, P.-H. C. Chen, et al. Artificial intelligence for diagnosis and Gleason grading of prostate cancer: the PANDA challenge. *Nature medicine* 2022 28, 154:163. DOI: 10.1038/s41591-021-01620-2.
- [3] J. H. Pedersen, H. Ashraf, A. Dirksen, et al. The Danish randomized lung cancer CT screening trial—overall design and results of the prevalence round. *Journal of Thoracic Oncology* 2009 4, 608:614. DOI: 10.1097/JTO.0b013e3181a0d98f.
- [4] D. Peeters, B. Obreja, N. Antonissen, and C. Jacobs. *The LUNA25 Challenge: Public Training and Development set - Annotation Data*. Version 1.0.0. Feb. 15, 2025. DOI: 10.5281/ZENODO.14673658. URL: <https://zenodo.org/doi/10.5281/zenodo.14673658> (visited on 10/31/2025).
- [5] Radboudumc. *LEOPARD Challenge. LEarning biOchemical Prostate cAncer Recurrence from histopathology sliDes (LEOPARD) challenge*. <https://leopard.grand-challenge.org>. Feb. 19, 2024. (Visited on 02/12/2025).
- [6] A. Saha, J. S. Bosma, J. J. Twilt, et al. Artificial intelligence and radiologists in prostate cancer detection on MRI (PI-CAI): an international, paired, non-inferiority, confirmatory study. *The Lancet Oncology* 2024 25, 879:887. DOI: 10.1016/S1470-2045(24)00220-1.
- [7] W. Hendrix, N. Hendrix, E. T. Scholten, et al. Deep learning for the detection of benign and malignant pulmonary nodules in non-screening chest CT scans. *Communications Medicine* 2023 3, p. 156. DOI: 10.1038/s43856-023-00388-5.
- [8] A. A. A. Setio, A. Traverso, T. de Bel, et al. Validation, comparison, and combination of algorithms for automatic detection of pulmonary nodules in computed tomography images: The LUNA16 challenge. *Medical Image Analysis* 2017 42, 1:13. DOI: 10.1016/j.media.2017.06.015.
- [9] M. van Rijthoven, W. Aswolinskiy, L. Tessier, et al. Tumor-infiltrating lymphocytes in breast cancer through artificial intelligence: biomarker analysis from the results of the TIGER challenge. *medRxiv* 2025. eprint: <https://www.medrxiv.org/content/early/2025/03/03/2025.02.28.25323078.full.pdf>.
- [10] M. de Grauw, E. Scholten, E. Smit, et al. The ULS23 challenge: A baseline model and benchmark dataset for 3D universal lesion segmentation in computed tomography. *Medical Image Analysis* 2025 102, p. 103525. ISSN: 1361-8415. DOI: 10.1016/j.media.2025.103525.
- [11] J. W. van der Graaf, M. L. van Hooff, C. F. Buckens, et al. Lumbar spine segmentation in MR images: a dataset and a public benchmark. *Scientific Data* 2024 11, p. 264. DOI: 10.1038/s41597-024-03090-w.
- [12] J. S. Bosma, K. Dercksen, L. Bultjes, et al. The DRAGON benchmark for clinical NLP. *npj Digital Medicine* 2025 8, 1:10. DOI: 10.1038/s41746-025-01626-x.
- [13] D. Carrell, B. A. Malin, J. S. Aberdeen, S. Bayer, C. R. Clark, B. Wellner, et al. Hiding in plain sight: use of realistic surrogates to reduce exposure of protected health information in clinical text. *Journal of the American Medical Informatics Association* 2013 20, 342:348. DOI: 10.1136/amiajnl-2012-001034.
- [14] W. Hendrix, M. Rutten, N. Hendrix, et al. Trends in the incidence of pulmonary nodules in chest computed tomography: 10-year results from two Dutch hospitals. *European radiology* 2023 33. DOI: 10.1007/s00330-023-09826-3.
- [15] M. D’Amato, R. Weber, J. Lefkes, et al. *The UNICORN Challenge: public few-shots*. Version 7.0. June 17, 2025. DOI: 10.5281/ZENODO.14832502. URL: <https://zenodo.org/doi/10.5281/zenodo.14832502> (visited on 11/07/2025).
- [16] K. V. Venkadesh, A. A. Setio, A. Schreuder, et al. Deep learning for malignancy risk estimation of pulmonary nodules detected at low-dose screening CT. *Radiology* 2021 300, 438:447. DOI: 10.1148/radiol.2021204433.
- [17] R. S. Vanguri, J. Luo, A. T. Aukerman, et al. Multimodal integration of radiology, pathology and genomics for prediction of response to PD-(L) 1 blockade in patients with non-small cell lung cancer. *Nature cancer* 2022 3, 1151:1164. DOI: 10.1038/s43018-022-00416-8.
- [18] Q. Da, X. Huang, Z. Li, et al. DigestPath: A benchmark dataset with challenge review for the pathological detection and segmentation of digestive-system. *Medical Image Analysis* 2022 80, p. 102485. DOI: 10.1016/j.media.2022.102485.

- [19] S. G. I. Armato, G. McLennan, L. Bidaut, et al. The Lung Image Database Consortium (LIDC) and Image Database Resource Initiative (IDRI): A Completed Reference Database of Lung Nodules on CT Scans. *Medical Physics* 2011 38, 915:931. DOI: 10.1118/1.3528204.
- [20] C. A. Bertram, M. Aubreville, C. Marzahl, A. Maier, and R. Klopfleisch. A large-scale dataset for mitotic figure assessment on whole slide images of canine cutaneous mast cell tumor. *Scientific data* 2019 6, p. 274. DOI: 10.1038/s41597-019-0290-4.
- [21] P. Chen, H. Li, C. Zhu, S. Zheng, Z. Shui, and L. Yang. WsiCaption: Multiple Instance Generation of Pathology Reports for Gigapixel Whole-Slide Images. *proceedings of Medical Image Computing and Computer Assisted Intervention*. Vol. LNCS 15004. 2024.